Available online at www.sciencedirect.com
SCIENCE DIRECT®
Engineering Fracture Mechanics 72 (2005) 617–629
Engineering Fracture Mechanics
www.elsevier.com/locate/engfracmech

The effect of crack surface interaction on the stress intensity factor in Mode III crack growth in round shafts

A. Vaziri [1], H. Nayeb-Hashemi *

Department of Mechanical, Industrial and Manufacturing Engineering, Northeastern University, Boston, MA 02115, USA

Received 29 May 2003; received in revised form 10 March 2004; accepted 31 March 2004
Available online 6 July 2004

Abstract

Turbine-generator shafts are often subjected to a complex transient torsional loading. Such transient torques may initiate and propagate a circumferential crack in the shafts. Mode III crack growth in turbo-generator shafts often results in a fracture surface morphology resembling a factory roof. The interaction of the mutual fracture surfaces results in a pressure and a frictional stress field between fracture surfaces when the shaft is subjected to torsion. This interaction reduces the effective Mode III stress intensity factor.

The effective stress intensity factor in circumferentially cracked round shafts is evaluated for a wide range of applied torsional loading by considering a pressure distribution between mating fracture surfaces. The pressure between fracture surfaces results from climbing of asperities respect to each other. The pressure profile not only depends on the fracture surface roughness (height and width (wavelength) of the peak and valleys), but also depends on the magnitude of the applied Mode III stress intensity factor. The results show that asperity interactions significantly reduce the effective Mode III stress intensity factor. However, the interactions diminish beyond a critical applied Mode III stress intensity factor. The critical stress intensity factor depends on the asperities height and wavelength. The results of these analyses are used to find the effective stress intensity factor in various Mode III fatigue crack growth experiments. The results show that Mode III crack growth rate is related to the effective stress intensity factor in a form of the Paris law.

Keywords: Turbo-generator shafts; Transient torsional loading; Circumferential crack; Crack growth; Crack surfaces interaction; Effective stress intensity factor

1. Introduction

Circumferential cracks may initiate and propagate in turbine-generator shafts as they are often subjected to a complex transient torsional loading (Mode III) [1]. The experimental investigations have shown that the Mode III crack growth in a shaft could be very tortures, resulting in a crack front segmentation, often

* Corresponding author. Tel.: +1-617-373-5515; fax: +1-617-373-2921.
E-mail address: hamid@coe.neu.edu (H. Nayeb-Hashemi).
[1] Current address: Division of Engineering and Applied Sciences, Havard University, Cambridge, MA 02138, USA.

0013-7944/$ - see front matter © 2004 Elsevier Ltd. All rights reserved.
doi:10.1016/j.engfracmech.2004.03.014

Nomenclature

a	radius of uncracked region
b	crack length
F	uniformly distributed dummy normal force at x_1
E'	material elastic constant
G	material shear modulus
h	asperity height
K_{eff}	effective stress intensity factor
K_{III}	applied stress intensity factor
K_{fric}	frictional stress intensity factor
R	shaft radius
T	applied torque
x_1	extent of the crack surface interaction
u_1	axial crack opening displacement at the point x_1
$u_3(x)$	Mode III crack displacement
α	asperity angle
μ	friction coefficient
λ	asperity wavelength
σ_0	normal stress at the crack tip, Case A
σ_y	material yield stress
Γ	effective frictional coefficient
$\mathscr{L}$	energy release rate

called a factory roof fracture surface. The fracture surface roughness depends on the material microstructure, the material yield strength, and the applied cyclic torque amplitude [1–12]. For a shaft subjected to high cyclic torque amplitude, the fracture surface is macroscopically flat. However, at low cyclic torque amplitude, the fracture surface consists of peaks and valleys resembling a factory roof. In contrast to Mode I crack growth, where there is little crack surface interaction, Mode III crack surfaces interact in a complicated manner. Crack surface interaction occurs when macroscopically rough crack surfaces are displaced relative to one another in shear. The contacting peaks and valleys of opposing crack surfaces interact through some combination of sliding, climbing, sticking, slipping and deforming [2]. Nayeb-Hashemi et al. [3,4] showed that Mode III crack growth rate could decrease substantially under a constant cyclic torque, in contrast to Mode I crack growth, which accelerates under a constant cyclic opening load. This was attributed to the change in the crack growth morphology, from a macroscopically flat fracture surface to a rough fracture surface, which causes the interaction of mating facture surfaces. In later papers [5,6], it was shown that superimposing a static axial load on the cyclic Mode III component decreased the crack surface interactions and increased the crack growth rate.

There are a number of papers on the criteria for the crack front segmentations for a cracked structure subjected to Mode I, II, and III loadings [13–16]. The simplest theory is that the crack front tends to rotate in the direction of maximum principal stress [13,14], Mode I direction. Lazarus et al. [15,16] in a series of papers developed criteria for crack front rotation and segmentation in brittle materials under mixed Mode I + III or I + II + III conditions. A qualitative explanation of segmentation in Mode I + III, based on the energetic theory of fracture was presented. It was shown that a suitable energy release rate criteria was able to predict the crack front rotation. However, they have apparently ignored the crack surfaces interactions in deriving the crack front rotation criteria. The crack front rotation could be obtained by considering the

superposition of applied Mode I and Mode I resulting from the crack surfaces interaction. Since the contribution of Mode I stress intensity factor stemming from the crack surface interactions changes during cyclic torsion, it is a difficult task to predict crack angle rotation using this theory.

Gross and Mendelsohn [17–19] developed an elastic plastic model to understand the crack surface interactions in Mode III crack growth. The normal contact pressure, which arises when the macroscopically rough fracture surfaces displace respect to each other, was obtained by modeling the crack surface interactions as edge dislocations. The pressure distribution along the crack surface was obtained by considering the crack opening in Mode I and the crack sliding in Mode III. The shear displacement of the crack surfaces along with the normal pressure result in a frictional torque, thus reducing the Mode III stress intensity factor at the crack tip. However, the proposed pressure distribution functions apparently result in a singular function and in some cases could not be utilized to find the normal pressure distribution on the crack surfaces.

The purpose of the work described in this paper is to obtain the effective Mode III stress intensity factor in circumferentially cracked shafts with a factory roof fracture surface subjected to a torsional loading. The model is based on a fracture surface covered with asperities with small height and wavelength. The analysis incorporates asperity-interlocking mechanism in determining the frictional Mode III stress intensity factor. Furthermore, the results of this investigation have been used in modeling the dynamic response of the cracked shafts subjected to cyclic torsion [20].

2. Theoretical investigation

Schematic diagram of a cylindrical bar with a circumferential crack subjected to a torque, T, is shown in Fig. 1. The shaft material is considered linear elastic–perfectly plastic. Fig. 2 shows a typical fracture surface pattern in a shaft with a circumferential crack when subjected to low and high cyclic torque amplitudes. At low cyclic Mode III stress intensity factor amplitude, the crack growth generates a factory

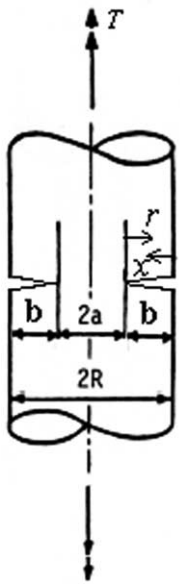

Fig. 1. Schematic model of a cylinder bar with a circumferential crack under torsion.

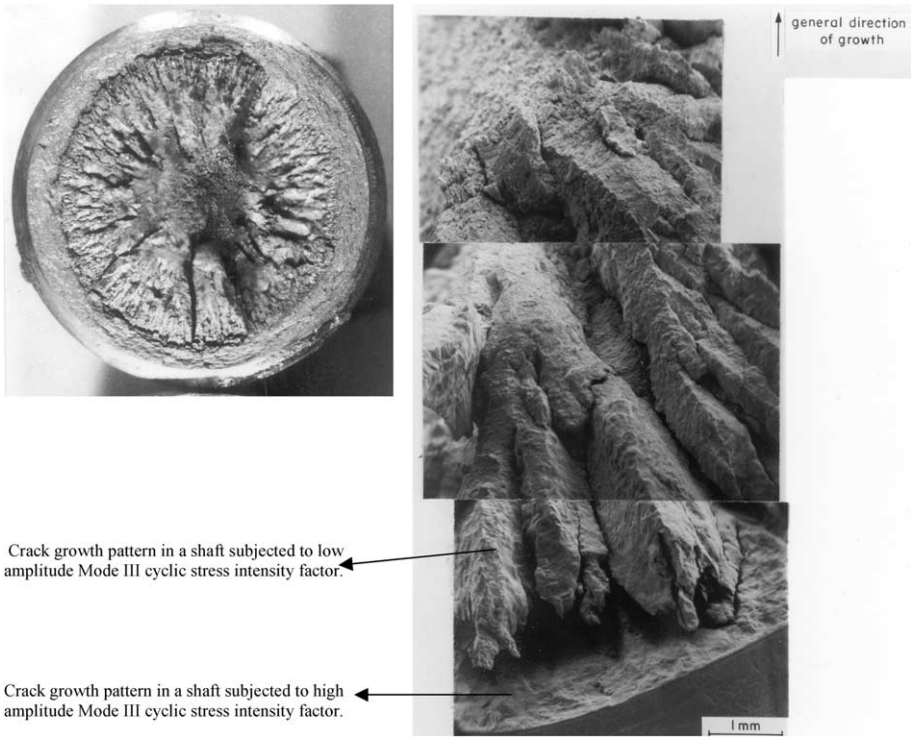

Fig. 2. Circumferential crack propagation pattern for a shaft under low and high applied Mode III stress intensity factor.

roof fracture surface. The height and wavelength of these asperities depend on the applied stress intensity factor, specimen geometry and material properties. This crack pattern results in interaction between crack surfaces, which decreases the effective stress intensity factor when the shaft is subjected to a torsional loading, Fig. 3. The effective stress intensity factor, K_{eff} can be stated as,

$$K_{\text{eff}} = K_{\text{III}} - K_{\text{fric}} \tag{1}$$

where K_{III} is the applied stress intensity factor by ignoring the crack surfaces interaction. K_{fric} is the frictional stress intensity factor, which is generated by the interaction of mating fracture surfaces. For a circumferentially cracked cylinder, K_{III} is given as [21],

$$K_{\text{III}} = \frac{2T\sqrt{1-\gamma}}{\sqrt{\pi}R^{2.5}\gamma^{2.5}}\left[1+\frac{1}{2}\gamma+\frac{3}{8}\gamma^2+\frac{5}{16}\gamma^3+\frac{35}{128}\gamma^4+0.208\gamma^5\right] \tag{2}$$

where

$$\gamma = \frac{a}{R} \tag{3}$$

In order to find the frictional stress intensity factor, the extent of the crack surface interaction, x_1 and resulted interaction pressure between mating fracture surfaces must be known, Fig. 4. The extent of the crack surface interaction depends on the applied torque amplitude and the asperity height and wavelength. For very small cyclic torque amplitude, the entire crack surfaces may interact. However, for larger torque amplitude only a segment of the crack may interact. The pressure distribution resulting from this interaction also depends on the asperities height and wavelength. Possible pressure profiles along the crack

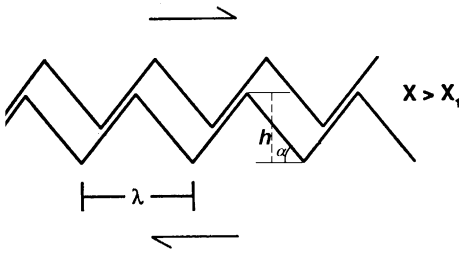

Fig. 3. Fracture surface profile for the Mode III crack displacement less than half of the asperities wavelength. (It is assumed that when the Mode III crack displacement is bigger than the half wavelength, there is no interaction between the crack surfaces.)

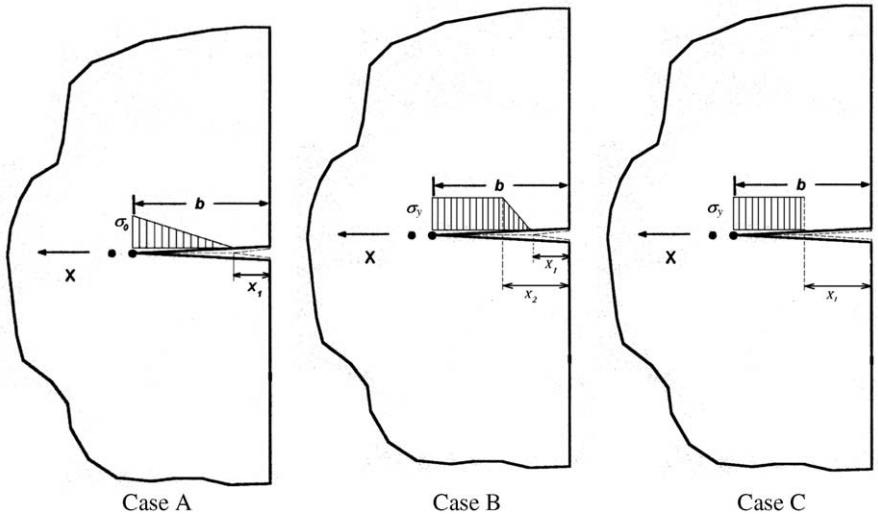

Fig. 4. Possible pressure distribution profiles between mating fracture surfaces, arising from the crack surface interactions.

surfaces are presented in Fig. 4. In Fig. 4A, it is assumed that the pressure varies linearly from the maximum at the crack tip to zero at $x = x_1$ and the maximum pressure is less than the material yield stress, σ_y. This assumption is based on the pervious investigations [19], which it was shown that the largest normal pressure developed very close to the crack tip. In this case, for the sake of simplicity, it is assumed pressure to vary linearly along the crack. For some asperities roughness and wavelength, the maximum pressure may become equal to the material yield stress. For this case the pressure distribution is assumed to be that of Fig. 4B. In this case, the pressure is equal to the material yield stress from the crack tip to a point, x_2, then it decreases linearly to zero at the point x_1. Fig. 4C indicates a uniform pressure distribution equal to the material yield stress. A particular pressure distribution depends on the applied torque and the fracture surface roughness. For small applied torques, the pressure distribution shown in Fig. 4A is expected to develop between the fracture surfaces. However, for high applied torques, the asperities are expected to slide over each other and may deform permanently, the pressure distribution shown in Fig. 4C is expected to develop between the fracture surfaces. For a moderate torque, the pressure distribution shown in Fig. 4B is expected to be present between the fracture surfaces. The extent of the crack surface interaction and the possible pressure profile could be evaluated by considering the crack opening and sliding displacements in Modes I and III. These could be obtained by considering that the Mode III crack displacement at the point

x_1 is equal to half wavelength, $\lambda/2$ (λ is the average wavelength, Fig. 3) and the crack opening displacement at this point is equal to the asperity height h. The Mode III crack displacement can be presented as [17],

$$u_3(x) = \frac{2K_{\text{eff}}}{G\sqrt{\pi b}}(b^2 - x^2)^{0.5} \tag{4}$$

The extent of the crack surface interaction, x_1, can be obtained from Eq. (4),

$$x_1 = b\sqrt{1 - \frac{\pi G^2 \lambda^2}{16K_{\text{eff}}^2}} \tag{5}$$

It is assumed that the there is no interaction between the crack surfaces for $x < x_1$. This assumption can be justified by considering that the Mode I displacement is greater than the asperity height for $x < x_1$. The frictional stress intensity factor can be evaluated from [18],

$$K_{\text{fric}} = -\left(\frac{b}{\pi}\right)^{0.5} \int_0^b \frac{\Gamma\sigma(x)}{(b^2 - x^2)^{0.5}}\,\mathrm{d}x \tag{6}$$

where $\sigma(x)$ is the pressure distribution between the fracture surfaces and Γ is the effective friction coefficient given as [18],

$$\Gamma = \frac{\tan\alpha + \mu}{1 - \mu\tan\alpha} \tag{7}$$

where μ is the friction coefficient between the sliding asperities and α is the asperity angle, defined in Fig. 3.

For a distributed pressure between the crack surfaces the crack opening displacement at the point x_1 is evaluated utilizing the Catligliano's theorem by applying a dummy uniform circumferential normal load at this point, Fig. 5. The energy release rate $\mathscr{L}$, can be presented as

$$\mathscr{L} = \frac{1}{E'}(K_{\text{IP}} + K_{\text{IF}})^2 \tag{8}$$

where K_{IP} is the stress intensity factor for the normal pressure distribution between the fracture surfaces and K_{IF} is the stress intensity factor for the circumferential distributed normal force F at x_1. E' is the elastic constant depending on the state of stress in the structure (plane stress or plane strain). The axial crack opening displacement at the point x_1 can be presented as,

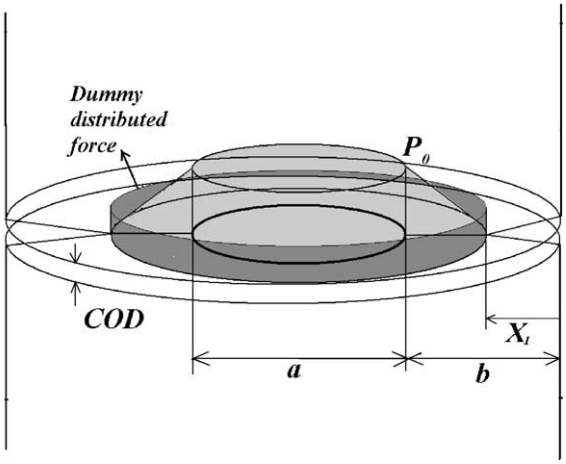

Fig. 5. Pressure distribution profile along with the circumferentially distributed normal dummy force, used to calculate the Mode I crack opening displacement utilizing the Catligliano's theorem.

$$u_1 = -\frac{2}{(R-x_1)E'}\left[\int_{x_1}^{b} \mathrm{d}x \int_{x}^{b} K_{\mathrm{IP}}(R-b)\left(\frac{\partial K_{\mathrm{IF}}}{\partial F}\right)\mathrm{d}b\right]_{F=0} \tag{9}$$

For a circumferentially cracked cylindrical bar, the stress intensity factors K_{IP} and K_{IF} are given as [21],

$$K_{\mathrm{IP}} = \frac{2\pi\sigma(x)(R-x)}{(\pi(R-b))^{1.5}}\left\{\cos^{-1}\frac{R-b}{R-x} + \frac{R-b}{\sqrt{(R-x)^2-(R-b)^2}}\right\} \tag{10}$$

and

$$K_{\mathrm{IF}} = \frac{2\pi F(R-x_1)}{(\pi(R-b))^{1.5}}\left\{\cos^{-1}\frac{R-b}{R-x_1} + \frac{R-b}{\sqrt{(R-x_1)^2-(R-b)^2}}\right\} \tag{11}$$

Substituting for the pressure distribution from Fig. 4A into Eq. (9) results in,

$$u_1 = -\frac{8\sigma_0}{\pi E'}\chi_1(R,b,x_1) \tag{12}$$

where $\chi_1(R,b,x_1)$ is defined in Eq. (A.2). σ_0 and x_1 can be evaluated by considering that, $u_1(x_1) = h$, and $u_3(x_1) = \lambda/2$.

$$\sigma_0 = -\frac{h\pi E'}{8\chi_1(R,b,x_1)} \tag{13}$$

The frictional stress intensity for this case can be presented as,

$$K_{\mathrm{fric}} = \left(\frac{b}{\pi}\right)^{0.5}\frac{h\pi E'\Gamma}{8\chi(R,b,x_1)(b-x_1)}\int_{x_1}^{b}\frac{(x-x_1)}{(b^2-x^2)^{0.5}}\mathrm{d}x \tag{14}$$

The crack opening displacement for the pressure distribution shown in Fig. 4B, can be presented as

$$u_1 = -\frac{8\sigma_{\mathrm{y}}}{\pi E'}\chi_2(R,b,x_1,x_2) \tag{15}$$

where x_1, and x_2 can be evaluated again by considering that $u_1(x_1) = h$, and $u_3(x_1) = \lambda/2$. The resisting stress intensity factor for this case is,

$$K_{\mathrm{fric}} = -\left(\frac{b}{\pi}\right)^{0.5}\Gamma\sigma_{\mathrm{y}}\left[\frac{1}{x_2-x_1}\int_{x_1}^{x_2}\frac{x-x_1}{(b^2-x^2)^{0.5}}\mathrm{d}x + \int_{x_2}^{b}\frac{1}{(b^2-x^2)^{0.5}}\mathrm{d}x\right] \tag{16}$$

For the pressure distribution shown in Fig. 4C, it is assumed that some of the asperities are deformed at relatively large Mode III displacement. For this case, the asperity height at point x_1 is unknown. However, the Mode III displacement is still equal to $\lambda/2$. The frictional stress intensity for this case can be presented as,

$$K_{\mathrm{fric}} = -\left(\frac{b}{\pi}\right)^{0.5}\Gamma\sigma_{\mathrm{y}}\int_{x_1}^{b}\frac{1}{(b^2-x^2)^{0.5}}\mathrm{d}x = -\left(\frac{b}{\pi}\right)^{0.5}\Gamma\sigma_{\mathrm{y}}\left(\frac{\pi}{2} - \arctan\left(\frac{x_1}{\sqrt{b^2-x_1^2}}\right)\right) \tag{17}$$

The pressure distribution parameters are obtained by simultaneously satisfying the Mode I crack opening displacement and Mode III crack displacement at the point x_1. This requires solution of a set of nonlinear equations. An algorithm is developed to solve these equations, Fig. 6. The pressure distribution parameters may not be found from this algorithm, if the applied torque is small. This may suggests that the

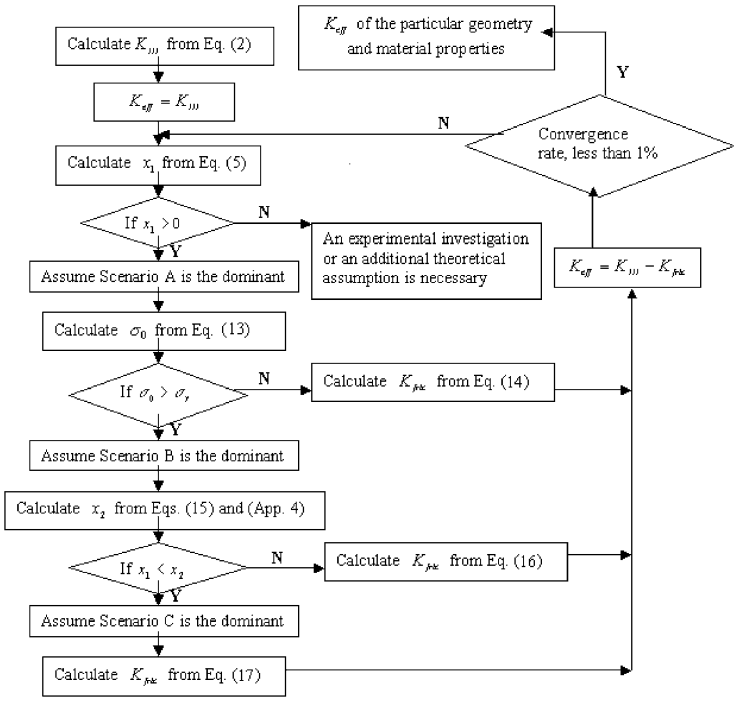

Fig. 6. Flow chart used to calculate Mode I and Mode III crack opening displacements and their convergence.

Mode III crack mouth displacement is less than half of the asperity wavelength. In this case, an experimental data regarding Mode III crack mouth displacement is required in order to obtain the pressure profile parameters. Since the set of equations for the Mode I and Mode III crack displacements are nonlinear, it is possible that the solution results in two possible pressure profiles (Cases A and B), Fig. 4. A conservative approach for estimating the fatigue life of a shaft should be based on a pressure profile with a lower frictional stress intensity factor.

3. Results and discussions

Table 1 shows the mechanical properties of the steel specimen used in this theoretical investigation. The effects of various geometrical parameters on the effective Mode III stress intensity factor are investigated for the shaft subjected to a wide range of applied Mode III stress intensity factor.

Fig. 7 shows the effective Mode III stress intensity factor vs. the applied (theoretical) Mode III stress intensity factor for a shaft with the radius of 10 cm and fracture surface roughness of $\lambda = 100$ μm and $h = 10$ μm. The results indicate that for the applied stress intensity factor of less than 50 MPa$\sqrt{\text{m}}$, the pressure interaction of the form presented in Fig. 4A is expected between mating fracture surfaces. The results also

Table 1
Material properties of models

Material	4140 steel, in annealed condition	Elastic modulus	200 GPa
Poisson's ratio	0.3	Yield stress	420 MPa

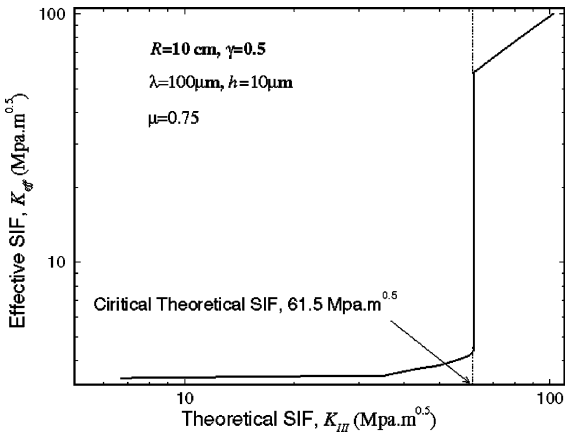

Fig. 7. Effective Mode III stress intensity factor vs. the applied Mode III stress intensity.

demonstrate a significant reduction in the applied stress intensity factor due to the crack surfaces interaction. This result is in agreement with the experimental data where it was observed that the crack growth rate progressively decreased despite of increasing the crack length, for a specimen subjected to constant cyclic torque amplitude [3,4]. For the applied stress intensity factor of 50–61.5 MPa$\sqrt{\text{m}}$, the pressure distribution shown in Fig. 4B governs the interaction pressure. The crack surfaces could be assumed interlocked as long as either x_1 or x_2 are less than the crack length (Fig. 4 (Cases A and B)) which results in a significant reduction in the effective stress intensity factor. For the applied stress intensity factor greater than 61.5 MPa$\sqrt{\text{m}}$, there is almost no interaction between fracture surfaces. It can be assumed that x_1 approaches the crack length. In this case, there is no locking mechanism preventing Mode III crack sliding. This results in a sudden burst in the Mode III crack sliding. Here again the experimental data shows a high crack growth rate for this range of applied stress intensity factor, indicating little crack surface interaction [4,5]. The critical stress intensity factor for no crack interaction depends on the asperities height and wavelength. Fig. 8 shows that the critical stress intensity factor decreases with reduction of the asperities height. The results also indicate that for an applied stress intensity factor of less than the critical stress intensity factor, the frictional stress intensity is moderately reduced with reduction of the asperity height.

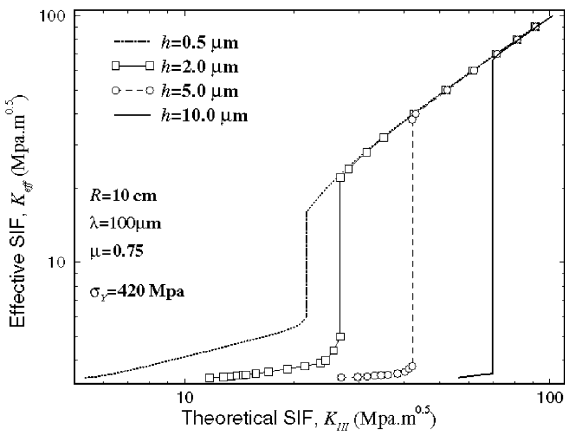

Fig. 8. Effective Mode III stress intensity factor vs. the applied Mode III stress intensity factor for various asperities heights.

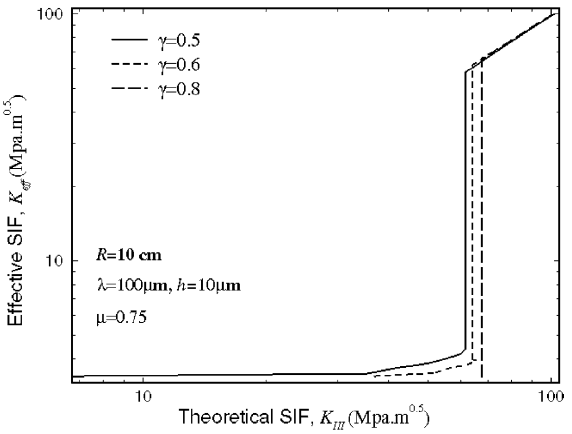

Fig. 9. Effective Mode III stress intensity factor vs. the applied Mode III stress intensity factor for various crack lengths.

The effect of the crack length on the critical stress intensity factor is shown in Fig. 9. The results show that the critical stress intensity factor is little sensitive to the crack length. This result could be justified by considering that the crack surface interaction effectively prevents the Mode III crack sliding, thus providing an interlocking mechanism between fracture surfaces, as if there is no crack. Furthermore the results indicate that for small crack length, the only way to open the crack surfaces more than the asperities height is by deforming the asperities. However, for a longer crack length, it is possible to open the crack surfaces more than the asperities height without deforming them.

The above analytical results are utilized to evaluate the effective Mode III stress intensity factor in AISI 4140 round specimens subjected to various cyclic torque amplitudes (Fig. 10). The detail of the experiment can be obtained in Nayeb-Hashemi et al. [3,4]. The corresponding fatigue crack growth rate data versus the applied stress intensity factor shows a chaotic trend [3,4]. However, using the above analyses, the same crack growth rate data versus the effective stress intensity factor exhibit the general Paris fatigue crack growth rate behavior (Fig. 10). As we mentioned before, the asperities height and wavelength depend on the applied stress intensity factor. Here, we used $\lambda = 100$ μm and $h = 10$ μm. These asperities dimensions are consistent with the observed asperities dimensions in the fatigue fracture surface of specimens subjected to

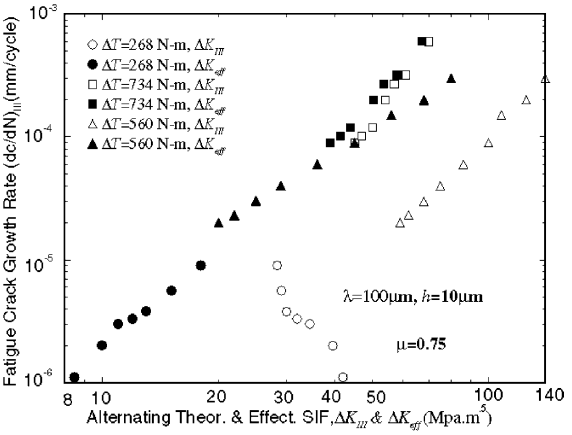

Fig. 10. Fatigue crack growth rate vs. the applied and effective Mode III stress intensity factors (Refs. [3,4]).

this range of applied stress intensity factor. The crack growth data is presented as a function of effective Mode III stress intensity factor rather than an effective crack driving force considering both Mode I and III stress intensity factors. This again could be justified considering that the experiments are conducted under cyclic torsion. Mode I is induced as a result of crack surface interactions. Since the material is elastic perfectly plastic, the normal stress in the plastic zone relaxes as the applied torque increases. This results in a damage mechanism at the crack tip which is mainly controlled by the cyclic torsion. For these reasons, we believed it is justified to consider effective Mode III stress intensity factor as the crack driving force.

4. Conclusions

The effects of Mode III crack surface interactions in circular shafts subjected to torsion on the effective stress intensity are investigated. The fracture surface is considered in a form of a factory roof, with asperities height of h and wavelength of λ. The mutual sliding interactions of these asperities results in a pressure and a frictional stress fields between fracture surfaces. Three cases of pressure distributions are taken into consideration. The pressure distribution parameters are obtained by considering both crack opening displacements in Mode I and III. Based on these analyses it was found:

1. Fracture surface interaction in circumferentially cracked shafts could result in a significant reduction in the effective Mode III stress intensity factor. The frictional stress intensity factor depends on the shaft radius, crack length, asperities height and wavelength and the shaft material properties.
2. The critical Mode III stress intensity factor is defined when asperities completely override each other. For applied Mode III stress intensity factors greater than this the critical value, there is a negligible crack surface interactions.
3. The critical stress intensity factor depends on the asperities height and wavelength. The critical stress intensity for complete sliding of the asperities over each other reduces with the reduction in the asperities height.
4. Mode III crack growth follows the Paris law when the effective stress intensity is considered in the crack driving force.

Appendix A

Case A. The normal stress is changing linearly from the maximum value of $\sigma_0 < \sigma_y$ at the crack tip to zero at x_1 (Fig. 4)

$$\sigma(x) = \begin{cases} 0, & 0 < x < x_1 \\ \sigma_0 \dfrac{x - x_1}{b - x_1}, & x_1 < x < b \end{cases} \tag{A.1}$$

$\chi_1(R, b, x_1)$ in this case can be calculated from,

$$\chi_1(R,b,x_1) = \left[\int_{x_1}^{b} (R-x)(x-x_1)\mathrm{d}x \int_{x}^{b} \frac{1}{(R-b)^2(b-x_1)} \left\{ \cos^{-1}\frac{R-b}{R-x_1} + \frac{R-b}{\sqrt{(R-x_1)^2-(R-b)^2}} \right\} \right.$$
$$\left. \times \left\{ \cos^{-1}\frac{R-b}{R-x} + \frac{R-b}{\sqrt{(R-x)^2-(R-b)^2}} \right\} \mathrm{d}b \right] \tag{A.2}$$

Case B. The normal stress is equal to the yield stress from the crack tip to a point at the distance x_2 from the crack tip from where it linearly decreases to zero at the point x_1.

$$\sigma(x)=\begin{cases}0, & 0<x<x_1\\ \sigma_y\dfrac{x-x_1}{x_2-x_1}, & x_1<x<x_2\\ \sigma_y, & x_2<x<b\end{cases} \tag{A.3}$$

$\chi_2(R,b,x_1,x_2)$ in this case can be calculated from,

$$\begin{aligned}\chi_2(R,b,x_1,x_2)=&\left[\int_{x_2}^{b}(R-x)\,\mathrm{d}x\int_{x}^{b}\frac{1}{(R-b)^2}\left\{\cos^{-1}\frac{R-b}{R-x_1}+\frac{R-b}{\sqrt{(R-x_1)^2-(R-b)^2}}\right\}\right.\\ &\times\left\{\cos^{-1}\frac{R-b}{R-x}+\frac{R-b}{\sqrt{(R-x)^2-(R-b)^2}}\right\}\mathrm{d}b+\int_{x_1}^{x_2}(R-x)(x-x_1)\,\mathrm{d}x\int_{x}^{b}\frac{1}{(R-b)^2(x_2-x_1)}\\ &\left.\times\left\{\cos^{-1}\frac{R-b}{R-x_1}+\frac{R-b}{\sqrt{(R-x_1)^2-(R-b)^2}}\right\}\left\{\cos^{-1}\frac{R-b}{R-x}+\frac{R-b}{\sqrt{(R-x)^2-(R-b)^2}}\right\}\mathrm{d}b\right]\end{aligned} \tag{A.4}$$

Case C. The normal stress is equal to the yield stress of the material along the interaction zone, x_1,

$$\sigma(x)=\begin{cases}0, & 0<x<x_1\\ \sigma_y, & x_1<x<b\end{cases} \tag{A.5}$$

References

[1] Hurd NJ, Irvine PhE. Smooth specimen fatigue lives and microcrack growth modes in torsion. ASTM Special Technical Publication. Multiaxial Fatigue, San Francisco, CA, USA. 1985. p. 267–84.
[2] Goulet RU, Gross TS, Mendelson DA. Evidence of fracture surface interference for cracks loaded in shear detected by phase-shifted speckle interferometry. Metall Mater Trans A 1996;27A:3853–60.
[3] Nayeb-Hashemi H, McClintock FA. Effects of friction and high torque on fatigue crack propagation in mode III. Metall Trans A (Phys Metall Mater Sci) 1982;13(12):2197–204.
[4] Nayeb-Hashemi H, McClintock FA, Ritchie RO. Micro-mechanical modeling of mode III fatigue crack growth in rotor steels. Int J Fract 1983;23(3):163–85.
[5] Ritchie RO, McClintock FA, Nayeb-Hashemi H, Rittler MA. Mode III fatigue crack propagation in low alloy steel. Metall Trans A (Phys Metall Mater Sci) 1982;13A(1):101–10.
[6] Nayeb-Hashemi H, McClintock FA. Influence of overloads and block loading sequences on mode III fatigue crack propagation in A469 Rotor Steel. Engng Fract Mech 1983;18(4):763–83.
[7] Tschegg EK. A contribution to mode III fatigue crack propagation. Mater Sci Engng 1983;59:127–36.
[8] Tschegg EK. The influence of the static I load mode and R ratio on mode III fatigue crack growth behavior in mild steel. Mater Sci Engng 1982;54:127–37.
[9] Hourlier F, Mclean D, Pineau A. Fatigue crack growth behavior of Ti–5Al–2. 5Sn Alloy under complex stress (mode I plus stead mode III). Met Technol 1978;5(5):154–8.
[10] Tschegg EK, Meyer HR, Czegley M, Stanzl SE. Influence of a constant mode III load on mode I fatigue crack growth thresholds. Fatigue Under Biaxial and Multiaxial Loading 1991:213.
[11] Tanaka K, Akiniwa Y. Fatigue crack propagation under mixed mode I and III loading. In: Proc of the 1996 4th Int Conf on Computer-Aided Assessment and Control. June 3–5 1996. Fukuoka, Japan. p. 153–67.

[12] Tanaka K, Akiniwa Y, Nakamura H. J-Integral approach to mode III fatigue crack propagation in steel under torsional loading. Fatigue Fract Engng Mater Struct 1996;19(5):571–9.
[13] Logsdon WA. Mixed mode interface fracture criteria. Acta Metall Mater 1990;38(12):2637–44.
[14] Magill MA, Zwerneman FJ. An analysis of sustained mixed mode fatigue crack growth. Engng Fract Mech 1997;56(1):9–24.
[15] Lazarus V, Leblond JB, Mouchrif SE. Crack front rotation and segmentation in mixed mode I + III or I + II + III. Part I: calculation of stress intensity factor. J Mech Phys Solids 2001;49:1399–420.
[16] Lazarus V, Leblond JB, Mouchrif SE. Crack front rotation and segmentation in mixed mode I + III or I + II + III. Part I: calculation of stress intensity factor. J Mech Phys Solids 2001;49:1421–30.
[17] Gross TS, Mendelsohn DA. On the effect of crack surface contact and friction due to fracture surface roughness in edge cracks subjected to external shear. Engng Fract Mech 1988;31(3):405–20.
[18] Gross TS, Mendelsohn DA. Mode I stress intensity factors induced by fracture surface roughness under pure mode III loading: Application to the effect of loading modes on stress corrosion crack growth. Metall Trans A 1989;20A:1989–99.
[19] Gross TS, Mendelsohn DA. An analysis of frictional effects on cylindrical mode III fatigue crack propagation specimens. Fatigue Fract Engng Mater Struct 1988;11(3):167–78.
[20] Vaziri A, Nayeb-Hashemi H, Hamidzadeh HR. The effects of the crack surfaces interaction and the crack tip plasticity on the dynamic response of the circumferentially cracked turbo generator shafts. ASME, November 15–21, 2003. Washington DC, USA.
[21] Tada H, Paris PC, Irwin GR. The stress analysis of crack handbook. 3rd ed. ASME Press; 2000.